

Topological surface states in strained Dirac semimetal thin films

Pablo Villar Arribi,¹ Jian-Xin Zhu,^{2,3} Timo Schumann,⁴ Susanne Stemmer,⁴ Anton A. Burkov,⁵ and Olle Heinonen^{1,*}

¹*Materials Science Division, Argonne National Laboratory, Lemont, Illinois 60439, USA*

²*Theoretical Division, Los Alamos National Laboratory, Los Alamos, New Mexico 87545, USA*

³*Center for Integrated Nanotechnologies, Los Alamos National Laboratory, Los Alamos, New Mexico 87545, USA*

⁴*Materials Department, University of California, Santa Barbara, CA 93106*

⁵*Department of Physics and Astronomy, University of Waterloo, Waterloo, Ontario, Canada N2L 3G1*

(Dated: June 19, 2020)

We computationally study the Fermi arc states in a Dirac semimetal, both in a semi-infinite slab and in the thin-film limit. We use Cd_3As_2 as a model system, and include perturbations that break the C_4 symmetry and inversion symmetry. The surface states are protected by the mirror symmetries present in the bulk states and thus survive these perturbations. The Fermi arc states persist down to very thin films, thinner than presently measured experimentally, but are affected by breaking the symmetry of the Hamiltonian. Our findings are compatible with experimental observations of transport in Cd_3As_2 , and also suggest that symmetry-breaking terms that preserve the Fermi arc states nevertheless can have a profound effect in the thin film limit.

The discovery of topologically non-trivial phases of matter has revolutionized the world of solid-state physics and materials science in the past decade. These systems exhibit new exotic electronic properties that are of great fundamental interest and also make them versatile for potential technological applications. Among these phases, the most important ones to date are topological insulators (TIs), Dirac semimetals (DSMs), and Weyl semimetals (WSMs)^{1–6}. A peculiar property of these systems is that they exhibit unusual surface states that are protected by symmetry or topology against perturbations^{7–12}. Also common to TIs, DSMs, and WSMs is that spin-orbit coupling is relatively strong and leads to band inversion in parts of the Brillouin zone.

DSMs have special points in the Brillouin zone where the valence and conduction bands touch. These points, known as Dirac points, are protected both by time-reversal symmetry (TRS) and inversion symmetry. Because TRS is respected, there is a double Kramer's degeneracy at the Dirac points, and near them, the electron dispersions are approximately described by the massless Dirac equation. The surface states in a DSM connect pairs of Dirac points in so-called Fermi arcs which, similar to the TI surface states, have specific spin-momentum locking.

The surface states in topological materials are of great interest since they have explicit coupling between momentum and spin (spin-momentum locking) which has as a consequence that transport in the surface states is dissipationless. Furthermore, the spin-momentum locking can be used to impart spin Hall torque or used in other spintronics applications^{13–18}, and magnetic WSMs with broken TRS can give rise to a high-temperature quantum anomalous Hall effect^{19,20}, which is of intense fundamental and practical interest. Because of the unique properties and great versatility of the Fermi arc states, it is important to understand how they respond to external perturbations, such as strain. Furthermore, quantum transport such as the quantum Hall effect or the quantum anomalous Hall effect is manifested when the bulk

states do not contribute to the transport^{19–21}. This can in principle be achieved by gapping out the bulk states by going to the extreme thin-film limit where quantum confinement leads to a discrete spectrum of gapped bulk states. However, Fermi arc states decay exponentially into the bulk with a decay length that diverges at the Dirac or Weyl nodes. As a DSM or WSM thin film is made thinner, the Fermi arc states on the two surfaces will couple. This brings up a very important question: what happens with the Fermi arc states in the thin film limit?

In our work, we use Cd_3As_2 as a model. This compound features a three-dimensional linear excitation spectrum near the Fermi level^{22–24}, high mobility carriers^{25,26}, and it turns out to be prototypical DSM²⁷: It only has two Dirac nodes near the Γ point in the first Brillouin zone, very close in energy to the Fermi surface, and the line connecting them is parallel to the crystallographic c -axis. The structure of Cd_3As_2 is rather complicated with a large unit cell. Thin films of this material can be grown along the $[112]$ direction (which yields a projection of the two Dirac nodes on the (112) surface) over different substrates with a similar lattice parameters^{28,29}. This induces strain that breaks C_4 symmetry around the crystallographic c -axis that protects the Dirac bulk states while inversion symmetry is preserved³⁰. However recent experiments suggest that Fermi arc states are present in these thin films^{21,31–35}, which brings up the question of how the Fermi arc states evolve from the semi-infinite case into the ultra-thin film limit in the presence of broken symmetries.

We model the energy dispersion relation around the Γ point with the following 4×4 Kane-Mele³⁶ Hamiltonian from Wang et al.³⁷ that has been previously used in this material:^{37,38}

$$H_1(\mathbf{k}) = \epsilon_0(\mathbf{k})\mathbf{I}_4 + H_2(\mathbf{k}), \quad (1)$$

where \mathbf{I}_4 is the 4×4 identity matrix,

$$H_2(\mathbf{k}) = \begin{pmatrix} M(\mathbf{k}) & Ak_+ & Dk_+ & B^*(\mathbf{k}) \\ Ak_- & -M(\mathbf{k}) & B^*(\mathbf{k}) & 0 \\ Dk_- & B(\mathbf{k}) & M(\mathbf{k}) & -Ak_- \\ B(\mathbf{k}) & 0 & -Ak_+ & -M(\mathbf{k}) \end{pmatrix}, \quad (2)$$

$\epsilon_0(\mathbf{k}) = C_0 + C_1k_z^2 + C_2(k_x^2 + k_y^2)$, $M(\mathbf{k}) = M_0 + M_1k_z^2 + M_2(k_x^2 + k_y^2)$, and $k_{\pm} = k_x \pm ik_y$. The Hamiltonian in Eq. (1) is written in a total angular momentum representation using a basis set $|S_{\frac{1}{2}}, \frac{1}{2}\rangle$, $|P_{\frac{3}{2}}, \frac{3}{2}\rangle$, $|S_{\frac{1}{2}}, -\frac{1}{2}\rangle$, $|P_{\frac{3}{2}}, -\frac{3}{2}\rangle$ times a plane wave $\exp(-i\mathbf{k} \cdot \mathbf{r})$ valid near the Γ point in the first Brillouin zone. This representation uses a coordinate system coincident with the tetragonal crystallographic axes a , a , and c . The parameter D in Eq. (2) breaks inversion symmetry, and we use here $B(\mathbf{k}) = b_1k_z$ which breaks the C_4 symmetry about the tetragonal c axis, as would a strain in the plane perpendicular to the c axis. We note that higher-order terms in $B(\mathbf{k})$, e.g., k_z^3 , are in principle allowed. Such terms preserve the C_4 symmetry and do not open a gap but modify the surface states. The Hamiltonian $H_1(\mathbf{k})$ has also been shown to exhibit a transition between two phases with different mirror Chern numbers³⁹, as $B(\mathbf{k})$ passes through zero, corresponding to going from compressive to tensile strain. We are ignoring high-order terms here as the fits to the calculated DFT bandstructure did not require them, and focus on compressive strain that breaks the C_4 symmetry. With $b_1 \neq 0$, a gap will open up at the Dirac nodes, and a mass will be introduced. Although more complex functional forms of $B(\mathbf{k})$ could be considered³⁷, we have only considered the simplest form that breaks C_4 symmetry. While parameters for the Hamiltonian in Eq. (1) have been published earlier^{37,38} we obtain our parameters by fitting the bulk dispersion relation along different momentum directions to the electronic band structure calculated within DFT for both unstrained and strained cases.

Details about the DFT calculations, the fitting process, and the obtained parameters A , C_0 , C_1 , C_2 , M_0 , M_1 , M_2 , and b_1 are presented in the Supplemental Material⁴⁰. We consider two cases: (i) the relaxed structure with the experimental lattice parameters (that we call “unstrained”), and (ii) a case with a -0.7% compressive strain applied along the a crystallographic axis (“strained”). We solve for the Fermi arc states by solving the determinantal equations that result from imposing the boundary conditions⁴¹ on a semi-infinite or finite-thickness slab (see Supplemental Material for details). We note that for the unstrained case, in which the C_4 symmetry around the crystallographic c axis is preserved, the band structure is gapless and has two Dirac nodes located at momenta $k_z^0 = \pm\sqrt{-M_0/M_1}$. In this case the result of the fit yields $b_1 = 0$, as expected. As soon as this parameter is non-zero, a non-trivial gap opens up in the bulk band structure.

Semi-infinite slab: In Fig. 1 we show the momenta of the Fermi arc states in a semi-infinite slab of Cd_3As_2 oriented

along the [112] crystallographic direction for different energies. We can see the evolution of the Fermi arc states in four different cases: two different values of the parameter D (which breaks inversion symmetry) for strained and unstrained systems. The value of D is added to the parameters obtained from the fits to the DFT bulk bands.

As D is increased from zero, inversion symmetry is broken. This lifts the Kramers degeneracy in the topologically trivial bulk bands. Interestingly, the Fermi arc states remain rather unchanged. For the unstrained case, we find a gapless bulk energy dispersion with two Dirac cones along the (k'_x, k'_y) direction, perpendicular to the [112] crystallographic direction. The main effect of strain is to open a gap in the bulk bands, while the Fermi arc states remain rather unchanged as a function of D in the case of semi-infinite slabs. It has been shown that Fermi arc states can survive under certain symmetry breakings provided the bulk states maintain mirror symmetries^{39,42}. This is the case here, in which the two mirror symmetries with planes along the lines $k'_y = \pm k'_x$ are preserved, despite the finite values of b_1 and D , thus ensuring the presence of the surface states in the gap.^{39,42,43}

The Fermi arc states also evolve in an interesting fashion as the bulk gap is opened. The set of two Fermi arcs that connect the two bulk Dirac cones in the unstrained gapless case only touch at the Dirac nodes forming an elliptical contour. As strain is applied and the bulk bands become gapped, this contour smoothly evolves into a closed loop that extends throughout the gap. This leads to a Dirac cone of surface states in the gap^{23,39}: Under strain the DSM transforms into a TI, and the Fermi arc states of the DSM have transformed to the TSSs of a TI. *Thin film limit:* In Fig. 2 we show the Fermi arc states for different thicknesses L as a function of the symmetry-breaking parameter D and of strain. As one would expect, for large values of L one recovers the same result as in the semi-infinite slab. We have confirmed this for $L = 500 \text{ \AA}$ (not shown).

As L is decreased, the Fermi arc states start to evolve until they disappear in the region of energy and momenta around the Dirac points. This happens for a thickness of around $L = 20 \text{ \AA}$ in the unstrained case and for a thickness below $L = 50 \text{ \AA}$ in the strained case. We can see in Fig. 2 how for the unstrained cases (a) and (b), for the same values of energy, the contours become smaller for lower values of L . As L is reduced, these contours will eventually disappear at that particular energy. In the strained case the situation is a little bit more complex. Surface states seem also to reappear at positive energies relative to the middle of the gap [$L = 70$ in Fig. Fig. 2 (c)]. As the thickness is increased one eventually recovers a cone of surface states, which resembles the behavior observed for the strained case in the semi-infinite slab.

We observe also how the effect of breaking inversion symmetry by setting $D \neq 0$ is very much more pronounced in thin films than in semi-infinite slabs, in which the Fermi arc state were barely changed by this perturbation. In thin films, breaking the Hamiltonian inversion

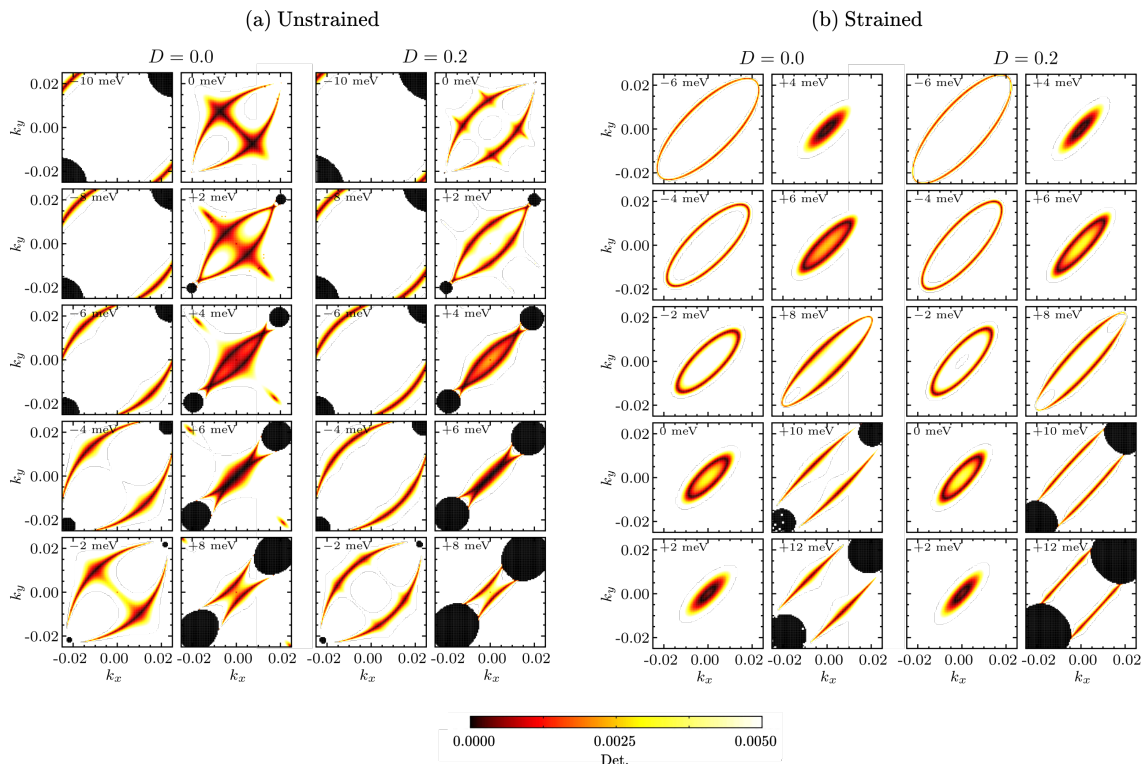


FIG. 1. Fermi arc states for a semi-infinite slab for the unstrained (a) and the strained case at -0.7% (b) and for two values of the inversion-symmetry-breaking parameter, $D = 0$ eV/Å and $D=0.2$ eV/Å. Units of k_x and k_y are Å⁻¹. The color scale indicates the numerical value of the determinant from the boundary condition. Inside each panel, we indicate the energy in meV with respect to the Dirac points (in the unstrained case) or to the gap center (strained case). The black areas correspond to the bulk states. The momenta (k_x, k_y) are perpendicular to the [112] crystallographic direction.

symmetry and lifting the Kramers degeneracy results in two sets of Fermi arc states that intersect or enclose each other. We believe this is a general feature of the Fermi arcs in the thin film limit and not limited to the specific model of Cd₃As₂ used here.

Interestingly, the thickness at which the Fermi arc states vanish completely is much smaller, around one order of magnitude, than the thinnest films fabricated so far (~ 100 Å), for which the dispersion of the Fermi arc states is practically identical to that in the semi-infinite slab. This allows to confirm that the Fermi arc states survive down to the extreme thin-film limit.

Moreover, the surface states survive in both unstrained and strained thin films, this is under broken inversion symmetry and broken C_4 symmetry along the crystallographic c -axis. It has been observed that the low-field-limit transport properties in Cd₃As₂ exhibit a strong anisotropy when the compound is grown along the [112] crystallographic direction³¹. The surface states will participate in transport and display the same type of symmetry as can be seen from the shape of the Fermi arc states, in particular in the range of energies immediately above and below the Dirac nodes. We speculate that this anisotropy of the surface states could be linked to the anisotropy seen in transport, although a more detailed

and thorough transport study is needed.

In addition, the strong particle-hole asymmetry and anisotropy of the surface states, especially in the thin film limit, will give rise to a rich variety of low-temperature transport properties. For example, with the chemical potential fixed, only Fermi arc states below it contribute to transport as the temperature is decreased, with the consequence that transport properties would smoothly develop a robust non-trivial contribution (as seen experimentally²⁹). Also, by effectively moving the chemical potential (by gating or by engineering heterostructures) the presence of surface states would become noticeable. Indeed, this has been observed experimentally³².

In general, the simplicity of the Dirac nodes and the robustness of the Fermi arc states in the thin-film limit and under different symmetry breakings investigated here, as well as experimentally^{21,31–33}, makes this material an ideal candidate for engineered heterostructures that probe transport that leverage the properties of Fermi arc states, such as the inverse Edelstein effect¹⁷, or spin-torque effects¹⁸.

We have also observed that varying the parameters of the model to values closer to those from Ref. 37, the results change. In particular the Fermi arc states remain in the thin film limit down to much thinner thicknesses

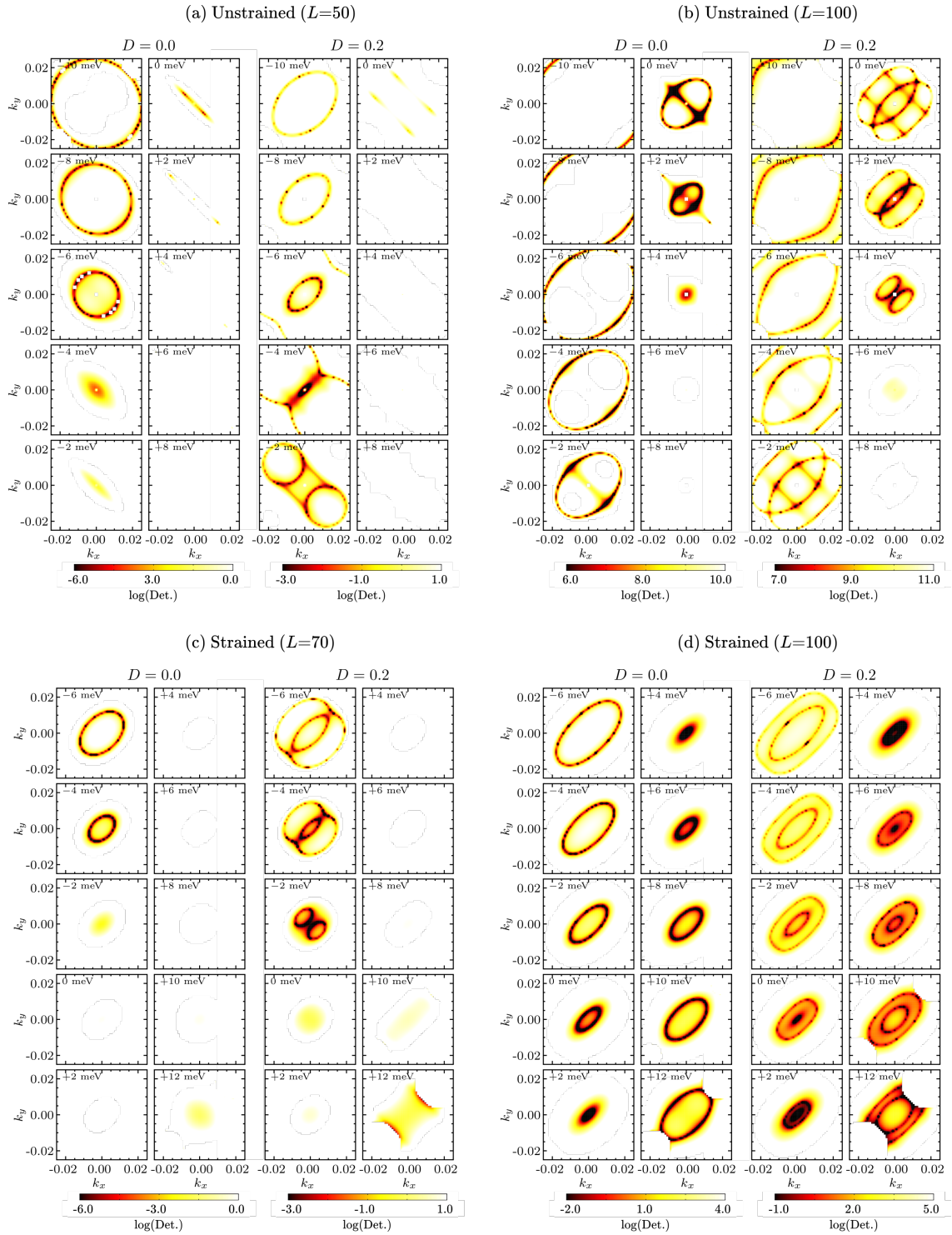


FIG. 2. Fermi arc states for several thin films in unstrained Cd_3As_2 (a),(b) and for the strained case at -0.7% (c),(d). For each of these cases we analyze two thicknesses ($L = 50, 100$, \AA for the unstrained case and $L = 70, 100$, \AA for the strained one), and two values of the inversion-symmetry-breaking parameter $D = 0.0, 0.2$ eV/ \AA . In color scale we plot the logarithm of the determinant of the boundary condition generalized to the thin film case. Inside each panel, we indicate the energy in meV with respect to the Dirac points (in the unstrained case) or to the gap center (strained and intermediate cases). The momenta (k_x, k_y) are perpendicular to the $[112]$ crystallographic direction.

(~ 5 \AA) whereas the behavior in the semi-infinite case is qualitatively similar, apart from an energy shift and

a reduction in the Lifshitz energy: the Fermi arc states are still present despite a relatively large difference in the parameters of the model, although its dispersion and low-energy features are different. This implies that the main results are not an artifact of our fit, although specific details in the thin-film limit are affected by the parameter choice.

In summary, we have studied the behavior of Fermi arc states in Cd_3As_2 both in a semi-infinite slab and in the thin film limit under strain and broken inversion symmetry. These Fermi arc states (arising from the linear combination of evanescent states satisfying the proper boundary conditions and protected by the presence of mirror symmetries in the bulk bands^{39,42,43}) survive to a film thickness below 50 \AA , smaller than presently reached experimentally, about 100 \AA ²⁹, and also survive under compressive strain, the only effect of which is to open

up a gap in the bulk bands both in the semi-infinite slab and in thin films (as has been observed experimentally³¹). Our findings are consistent with several experimental observations^{21,31–33}. Although we used specifically Cd_3As_2 as a model system, our approach using ab-initio determined parameters in conjunction with this four-band model can be generally applied to other candidate DSMs and WSMs. Breaking inversion symmetry in the Hamiltonian results in two sets of Fermi arc states in the thin film limit. We speculate that this is a general feature that will occur in other DSMs and is in principle observable.

This work was supported the Center for the Advancement of Topological Semimetals, an Energy Frontier Research Center funded by the U.S. Department of Energy Office of Science, Office of Basic Energy Sciences.

-
- * heinonen@anl.gov
- ¹ N. P. Armitage, E. J. Mele, and A. Vishwanath, *Rev. Mod. Phys.* **90**, 015001 (2018).
 - ² Z. Wang, Y. Sun, X.-Q. Chen, C. Franchini, G. Xu, H. Weng, X. Dai, and Z. Fang, *Phys. Rev. B* **85**, 195320 (2012).
 - ³ S. M. Young, S. Zaheer, J. C. Y. Teo, C. L. Kane, E. J. Mele, and A. M. Rappe, *Phys. Rev. Lett.* **108**, 140405 (2012).
 - ⁴ X. Wan, A. M. Turner, A. Vishwanath, and S. Y. Savrasov, *Phys. Rev. B* **83**, 205101 (2011).
 - ⁵ G. Xu, H. Weng, Z. Wang, X. Dai, and Z. Fang, *Phys. Rev. Lett.* **107**, 186806 (2011).
 - ⁶ B. Q. Lv, H. M. Weng, B. B. Fu, X. P. Wang, H. Miao, J. Ma, P. Richard, X. C. Huang, L. X. Zhao, G. F. Chen, Z. Fang, X. Dai, T. Qian, and H. Ding, *Phys. Rev. X* **5**, 031013 (2015).
 - ⁷ M. Z. Hasan and C. L. Kane, *Rev. Mod. Phys.* **82**, 3045 (2010).
 - ⁸ A. Bansil, H. Lin, and T. Das, *Rev. Mod. Phys.* **88**, 021004 (2016).
 - ⁹ C. L. Kane and E. J. Mele, *Phys. Rev. Lett.* **95**, 146802 (2005).
 - ¹⁰ B. A. Bernevig, T. L. Hughes, and S.-C. Zhang, *Science* **314**, 1757 (2006).
 - ¹¹ L. Fu, C. L. Kane, and E. J. Mele, *Phys. Rev. Lett.* **98**, 106803 (2007).
 - ¹² J. E. Moore and L. Balents, *Phys. Rev. B* **75**, 121306(R) (2007).
 - ¹³ I. M. Miron, K. Garello, G. Gaudin, P.-J. Zermatten, M. V. Costache, S. Auffret, S. Bandiera, B. Rodmacq, A. Schuhl, and P. Gambardella, *Nature* **476**, 189 (2011).
 - ¹⁴ L. Liu, C.-F. Pai, Y. Li, H. Tseng, D. Ralph, and R. Buhrman, *Science* **336**, 555 (2012).
 - ¹⁵ N. H. D. Khang, Y. Ueda, and P. N. Hai, *Nature Materials* **17**, 808 (2018).
 - ¹⁶ D. Mahendra, R. Grassi, J.-Y. Chen, M. Jamali, D. R. Hickey, D. Zhang, Z. Zhao, H. Li, P. Quarterman, Y. Lv, *et al.*, *Nature Materials* **17**, 800 (2018).
 - ¹⁷ S. S.-L. Zhang, A. A. Burkov, I. Martin, and O. G. Heinonen, *Phys. Rev. Lett.* **123**, 187201 (2019).
 - ¹⁸ P. Li, J. Kally, S. S.-L. Zhang, T. Pillsbury, J. Ding, G. Csaba, J. Ding, J. Jiang, Y. Liu, R. Sinclair, *et al.*, *Science Advances* **5**, eaaw3415 (2019).
 - ¹⁹ C.-X. Liu, X.-L. Qi, X. Dai, Z. Fang, and S.-C. Zhang, *Physical Review Letters* **101**, 146802 (2008).
 - ²⁰ C.-Z. Chang, J. Zhang, X. Feng, J. Shen, Z. Zhang, M. Guo, K. Li, Y. Ou, P. Wei, L.-L. Wang, *et al.*, *Science* **340**, 167 (2013).
 - ²¹ T. Schumann, L. Galletti, D. A. Kealhofer, H. Kim, M. Goyal, and S. Stemmer, *Phys. Rev. Lett.* **120**, 016801 (2018).
 - ²² S. Borisenko, Q. Gibson, D. Evtushinsky, V. Zabolotnyy, B. Büchner, and R. J. Cava, *Phys. Rev. Lett.* **113**, 027603 (2014).
 - ²³ H. Yi, Z. Wang, C. Chen, Y. Shi, Y. Feng, A. Liang, Z. Xie, S. He, J. He, Y. Peng, *et al.*, *Scientific Reports* **4**, 6106 (2014).
 - ²⁴ Z. Liu, J. Jiang, B. Zhou, Z. Wang, Y. Zhang, H. Weng, D. Prabhakaran, S. Mo, H. Peng, P. Dudin, *et al.*, *Nature Materials* **13**, 677 (2014).
 - ²⁵ A. J. Rosenberg and T. C. Harman, *Journal of Applied Physics* **30**, 1621 (1959).
 - ²⁶ M. Neupane, S.-Y. Xu, R. Sankar, N. Alidoust, G. Bian, C. Liu, I. Belopolski, T.-R. Chang, H.-T. Jeng, H. Lin, *et al.*, *Nature Communications* **5**, 1 (2014).
 - ²⁷ I. Crassee, R. Sankar, W.-L. Lee, A. Akrap, and M. Orlita, *Phys. Rev. Materials* **2**, 120302 (2018).
 - ²⁸ T. Schumann, M. Goyal, H. Kim, and S. Stemmer, *APL Materials* **4**, 126110 (2016), <https://doi.org/10.1063/1.4972999>.
 - ²⁹ M. Goyal, L. Galletti, S. Salmani-Rezaie, T. Schumann, D. A. Kealhofer, and S. Stemmer, *APL Materials* **6**, 026105 (2018), <https://doi.org/10.1063/1.5016866>.
 - ³⁰ T. Pardue, T. Schumann, and S. Stemmer, "(private communication)".
 - ³¹ M. Goyal, H. Kim, T. Schumann, L. Galletti, A. A. Burkov, and S. Stemmer, *Phys. Rev. Materials* **3**, 064204 (2019).
 - ³² L. Galletti, T. Schumann, O. F. Shoron, M. Goyal, D. A. Kealhofer, H. Kim, and S. Stemmer, *Phys. Rev. B* **97**, 115132 (2018).
 - ³³ L. Galletti, T. Schumann, T. E. Mates, and S. Stemmer,

- [Phys. Rev. Materials **2**, 124202 \(2018\)](#).
- ³⁴ C. Zhang, A. Narayan, S. Lu, J. Zhang, H. Zhang, Z. Ni, X. Yuan, Y. Liu, J.-H. Park, E. Zhang, *et al.*, *Nature Communications* **8**, 1 (2017).
- ³⁵ M. Uchida, Y. Nakazawa, S. Nishihaya, K. Akiba, M. Kriener, Y. Kozuka, A. Miyake, Y. Taguchi, M. Tokunaga, N. Nagaosa, *et al.*, *Nature Communications* **8**, 1 (2017).
- ³⁶ C. L. Kane and E. J. Mele, [Phys. Rev. Lett. **95**, 226801 \(2005\)](#).
- ³⁷ Z. Wang, H. Weng, Q. Wu, X. Dai, and Z. Fang, [Phys. Rev. B **88**, 125427 \(2013\)](#).
- ³⁸ S. Jeon, B. B. Zhou, A. Gyenis, B. E. Feldman, I. Kimchi, A. C. Potter, Q. D. Gibson, R. J. Cava, A. Vishwanath, and A. Yazdani, *Nature Materials* **13**, 851 (2014).
- ³⁹ G. Bednik, [Phys. Rev. B **98**, 045140 \(2018\)](#).
- ⁴⁰ See Supplemental Material at XXX.
- ⁴¹ K. Hashimoto, T. Kimura, and X. Wu, *Progress of Theoretical and Experimental Physics* **2017**, 053I01 (2017).
- ⁴² M. Kargarian, M. Randeria, and Y.-M. Lu, *Proceedings of the National Academy of Sciences* **113**, 8648 (2016).
- ⁴³ B.-J. Yang and N. Nagaosa, *Nature Communications* **5**, 1 (2014).